ORIGINAL RESEARCH

Mesoporous Calcium-Silicate Nanoparticles Loaded with Prussian Blue Promotes Enterococcus Faecalis Ferroptosis-Like Death by Regulating Bacterial Redox Pathway ROS/GSH

Xiao Zhao[1–3],*, Ying Wang[1–4],*, Tingting Zhu[1–3], Huili Wu[1–3], Diya Leng[1–3], Zhiguo Qin[5], Yan Li [6], Daming Wu[1–3]

[1]Department of Endodontics, the Affiliated Stomatological Hospital of Nanjing Medical University, Nanjing, People's Republic of China; [2]Jiangsu Province Key Laboratory of Oral Diseases, Nanjing, People's Republic of China; [3]Jiangsu Province Engineering Research Center of Stomatological Translational Medicine, Nanjing, People's Republic of China; [4]Nanjing Stomatological Hospital, Medical School of Nanjing University, Nanjing, People's Republic of China; [5]Nanjing Medical University, the First Clinical Medical College, Jiangsu Province Hospital, Nanjing, People's Republic of China; [6]State Key Laboratory of Bioelectronics, Jiangsu Key Laboratory for Biomaterials and Devices, School of Biological Science and Medical Engineering, Southeast University, Nanjing, People's Republic of China

*These authors contributed equally to this work

Correspondence: Daming Wu, Department of Endodontics, the Affiliated Stomatological Hospital of Nanjing Medical University, Jiangsu Province Key Laboratory of Oral Diseases, Jiangsu Province Engineering Research Center of Stomatological Translational Medicine, 1 Shanghai Road, Nanjing, 210029, People's Republic of China, Tel +086 025-69593056, Fax +086 025-86516414, Email wdming@njmu.edu.cn

Background: Mesoporous calcium-silicate nanoparticles (MCSNs) are advanced biomaterials that have been used to control drug delivery for many years. Ultrasmall Prussian blue nanoparticles (UPBNPs) showed high peroxidase and catalase-like activities. This study evaluated the antibacterial and antibiofilm properties, mechanism and cytotoxicity of UPBNPs-MCSNs composites synthesized by both as precursors.

Methods: UPBNPs-MCSNs were prepared and characterized. The antibacterial effect of UPBNPs-MCSNs was evaluated by the MTT assay and CFU counting method, and their biosafety was tested by CCK8. Then explore the antibacterial mechanism, including TEM observation of bacterial morphology, and detection of bacterial ROS, LPO and GSH levels. The antibiofilm activity of UPBNPs-MCSNs was tested by *E. faecalis* biofilm model in human roots. The roots were pretreated with materials and cultured with *E. faecalis*, and the survival of *E. faecalis* on the root canal wall was observed by SEM and CLSM.

Results: The results showed that UPBNPs-MCSNs had potent antibacterial and antibiofilm activities. They can aggregate on the dentin surface and significantly inhibit *E. faecalis* adhesion and colonization. Their antibacterial activity is as effective as NaClO and calcium hydroxide (CH), can significantly prolong the time of bacterial colonization than CH, but have lower cytotoxicity to normal cells. We found that UPBNPs-MCSNs trigger a like classic ferroptosis pathway in bacteria. UPBNPs-MCSNs can induce bacteria to produce ROS and LPO, and reduce GSH level. Moreover, we observed that the metal ions chelator and the antioxidant could block their antibacterial activity.

Conclusion: These results reveal that UPBNPS-MCSNs have high antibacterial and antibiofilm, and can mediate the bacterial redox pathway ROS/GSH like the classical pathway of ferroptosis, providing a theoretical basis for them to develop into a safe and effective novel root canal disinfectant.

Keywords: antibacterial activity, root canal disinfectant, mesoporous materials, reactive oxygen species, Prussian blue

Introduction

Periapical periodontitis (AP) is a common oral disease, an inflammatory bone destruction disease caused by the imbalance between the microbes and host immune responses.[1] If the microbes are not well controlled, AP can develop into persistent

periapical periodontitis (PAP), which makes it more difficult to treat.[2] Root canal therapy is internationally recognized as the first choice at present, but there is still a failure rate of 7% and 14%, secondary root canal treatment had an even lower success rate of 77%.[3–5] *Enterococcus faecalis* (*E. faecalis*) is the bacteria with the highest detection rate in the cases of failed root canal therapy, and it is also the most important pathogen in the progression of PAP, it has cytolysin, adhesive protein, gelatinase, lipoteichoic acid (LTA) and other virulence factors.[6,7] *E. faecalis* can form biofilm in the root canal wall, apical triangle, apical divergence and bifurcated root canal. Even with chemical and mechanical preparation, it is challenging to remove *E. faecalis* completely. *E. faecalis* can invade dentin tubules, tolerate antibiotics, oligotrophic and high alkaline (pH>11.5) environments, and survives in the state of persistor bacteria.[8] Therefore, long-term colonization of *E. faecalis* in periapical tissues brings excellent challenges to healing periapical lesions.

Mesoporous calcium-silicate nanoparticles (MCSNs) are a new kind of calcium silicate-based nano-biomaterials with ordered mesoporous structure (average 5 nm) and high specific surface area (average 300 m^2/g). MCSNs can release Ca^{2+} and SiO_4^{4-} in the liquid continuously, promote the formation of apatite mineralization and induce significant protein expression of periodontal ligament stem cells in the direction of tooth/bone differentiation.[9] The characteristic mesoporous structure of MCSNs can carry and continuously release metal ions, antibiotics and chemical drugs, showing suitable antibacterial properties,[10–12] which make MCSNs become excellent biological carriers. Our previous studies also found that MCSNs loaded with silver (Ag) and zinc (Zn) (Ag-Zn-MCSNs) damaged the membrane of *E. faecalis* by releasing silver nanoparticles (AgNPs), resulting in bacterial death. Its destruction effect of biofilm was significantly stronger than that of calcium hydroxide (CH), and the antimicrobial performance increased with the increase of Ag content, and the cytotoxicity decreased with the increase of Zn content.[11,12] Ag-Zn-MCSNs can enter the dentin tubule through ultrasonic shock, and the mechanical strength of dentin does not reduce after 30 days of endodontic sealing.[12,13]

Prussian blue (PB) is a kind of porous network cubic metal-organic framework ($Fe_4[Fe(CN)_6]_3$), which is composed of Fe (II) and Fe (III) and cyanide (-CN-) group.[14] It has excellent electrochemical and optical properties.[15] As a result of its specific ion exchange, adsorption, and mechanical capture characteristics, it was approved in 2003 by the US FDA as an antidote to thallium and cesium contamination in vivo. Prussian blue nanoparticles (PBNPs) are smaller and have a larger surface-volume ratio and porosity. The porosity and surface modifiability of PBNPs overcome the shortcomings of poor solubility, lack of target specificity and systemic toxicity of traditional drugs, and have the advantages of superior nano enzyme activity, magnetic, optical and electrochemical properties.[16] Our previous studies synthesized ultrasmall PBNPs (UPBNPs) (diameter 3.4 nm), showing a large specific surface area, high peroxidase and catalase-like activities and MRI imaging effect.[17] Li et al found that Zn^{2+}, Fe^{2+} and Fe^{3+} released by Zn-loaded PBNPs under infrared irradiation could quickly penetrate bacteria, interfere with bacterial intracellular metabolic pathway, improve bactericidal efficiency and have no systemic toxicity.[18] Shen et al found that multi-functionalized iron oxide nanoparticles selectively inhibit intracellular bacteria by releasing Fe^{2+} and Fe^{3+}, triggering lipid peroxidation and respiratory chain inhibition inducing ferroptosis-like death of bacteria.[19]

In this context, we used the template method to synthesize MCSNs, and then successfully prepared nanocomposites (UPBNPs-MCSNs) loaded with UPBNPs into MCSNs by a mixing-coupling method (The mass ratio of UPBNPs to MCSNs is 1:50). As PB acts as a potential exogenous iron pool, it is rich in Fe^{2+} and Fe^{3+}.[20] Due to the successful loading of iron ions, UPBNPs-MCSNs showed significantly better antibacterial properties against *E. faecalis* and *Streptococcus mutans (S. mutans)* than UPBNPs and MCSNs alone, and the toxicity was lower than that of silver ions. When exploring the mechanism, we found that UPBNPs-MCSNs can increase reactive oxygen species (ROS) and lipid peroxides (LPO) in bacteria and reduce the level of glutathione (GSH), that is, an imbalance in the antioxidant system that like the classical pathway of ferroptosis (GPX4/GSH axis is one of the classical pathways to regulate ferroptosis), which lays the foundation for the following discussion. Ferroptosis, a newly discovered regulatory cell death, is an iron-dependent nonapoptotic form of cell death.[21] Here, we report for the first time that ferroptosis is involved in the death of *E. faecalis* and its biofilm promoted by UPBNPs-MCSNs through the bacterial redox pathway ROS/GSH. This research intends to explore the antibacterial activity of UPBNPs-MCSNs on *E. faecalis* and its biofilm and to evaluate its antibacterial mechanism to provide an experimental basis for developing a safe and effective novel root canal disinfectant.

Materials and Methods

Synthesis and Characterization of the UPBNPs-MCSNs

The synthesis and characterization of MCSNs and UPBNPs have been mentioned in our previous studies.[7,13] UPBNPs and MCSNs were added to deionized water at a mass ratio of 1:50. After thoroughly mixed, the mixture was freeze-dried to obtain UPBNPs-MCSNs.

The UPBNPs-MCSNs were characterized by scanning electron microscopy (SEM, JSM-7900F, JEOL, Tokyo, Japan), transmission electron microscopy (TEM, Talos F200X, Thermo Fisher Scientific, Waltham, MA, USA) and energy dispersive spectrometry (EDS, X-Max50, Oxford Instruments, Abingdon, UK). Brunauer-Emmett-Teller (BET) and Barrett-Joyner-Halenda (BJH) methods (ASAP 2640, Micromeritics, Norcross, GA, USA) were used to investigate the surface area and pore distribution of MCSNs and UPBNPs-MCSNs. Through X-ray photoelectron spectroscopy (XPS, K-Alpha, Thermo Fisher Scientific, Waltham, MA, USA), Fourier transformed infrared spectroscopy (FT-IR, Nicolet iS10, Thermo Fisher Scientific, Waltham, MA, USA) and thermogravimetric analysis / differential thermal analysis (TGA / DTA, DTG-60H, Shimadzu, Japan) to evaluate the combination between MCSNs and UPBNPs, and thermal stability. The pH value of UPBNPs-MCSNs in deionized water was measured by a pH meter (SIN-PH100, Sinomeasure, China), and Iron Assay Kit (Sigma-Aldrich, St. Louis, MO, USA) measured the iron ion release curve.

Antibacterial Activity of the UPBNPs-MCSNs Detected by MTT Assay

UPBNPs-MCSNs was mixed with 250 μL *E. faecalis* (ATCC 29212, Manassas, VA, USA) suspension (OD600 =1) make the final concentration 2.5, 5, 10 and 20 mg/mL, respectively. Negative control was performed using Brain heart infusion (BHI, Oxoid, Basingstoke, UK), and positive control was performed using 1% NaClO (Langli Biological Medicine Co., Ltd., Wuhan, China). 37°C, 24 hours after anaerobic incubation, 50 μL MTT (Beyotime, Shanghai, China) was added to each group and cultured under dark conditions for 2 hours. Other initial groups were prepared according to the above method, and MTT was immediately added and cultured for 2 hours under dark conditions.

Then, each coculture was centrifuged at 10,000 r for 1 min, and the supernatant was discarded. 250 μL DMSO (Aladdin, Shanghai, China) was added and thoroughly shaken evenly to ensure the precipitated formazan fully dissolved. 200 μL blue-purple supernatant was taken after centrifuged at 10,000 r for 1 min. Absorption was measured with a microplate reader at 490 nm. Each group was tested 6 times with 3 wells.

Antibacterial Effects of the UPBNPs-MCSNs Detected by CFU Counting Method

The suspension of *E. faecalis* was gradient diluted to 1×10^4 CFUs/mL, and then UPBNPs-MCSNs were added to make the final concentration 2.5, 5 and 10 mg/mL, respectively. In addition, UPBNPs and MCSNs were added to make the final concentration 0.2 and 10 mg/mL (which is the component of the synthesis of 10mg/mL UPBNPs-MCSNs). Negative control was performed using bacteria, and positive control was performed using 1% NaClO and Calcium hydroxide (CH). In the same system, the final concentration of UPBNPs-MCSN was 10mg/mL, and then different concentrations of metal ions chelator ethylene diamine tetra acetic acid (EDTA; 5, 10, 20μM) (99.5%, Nanjing Ningshi Chemical Reagent Co., Ltd., China) and antioxidant ascorbic acid (Vc; 0.1, 1, 10 mg/mL) (99.0%, Beijing Zhongsheng Ruitai Technology Co., Ltd., China) were added. Bacteria were used as a negative control, and without EDTA and Vc as the positive control. 4°C, 24 hours anaerobic incubation. Then, 10 μL inoculums were coated on a BHI agar (Oxoid, Hampshire, UK) plate, and 37°C, 24 hours of anaerobic incubation. The CFU was counted using an automated collection counter (Scan 1200, Interscience, France). Each group was tested 6 times.

To further test the antibacterial activity of UPBNPs-MCSNs, we use similar methods mentioned above. The suspension of *S. mutans* (ATCC25175, Manassas, VA, USA) was diluted to $1 \times 10^4 \sim 1 \times 10^5$ CFU/mL and co-cultured with 0.2mg/mL UPBNPs, 10 mg/mL MCSNs and 10 mg/mL UPBNPs-MCSNs for 4°C, 24 h anaerobic incubation. Similarly, 10 μL inoculums were coated on a BHI agar plate and incubated anaerobically at 37°C for 36 h. Each group was tested 6 times.

Biosafety of the UPBNPs-MCSNs

Impacted teeth of healthy children were collected according to the approval of the Ethical Committee Department, the Affiliated Stomatological Hospital of Nanjing Medical University (PJ2020-128-001). The apical papilla tissue was cut and digested by trypsin and collagenase. Then, the digestion was terminated after incubating for 20 mins. The cells were centrifuged, cultured and subcultured in the petri dish. The third generation SCAPs with good growth condition and cell identification was used in the experiment.

SCAPs seeded in wells at a density per well is $2*10^3$ were inoculated in α-MEM medium (Gibco, Grand Island, USA) containing 10% FBS (Invitrogen, Carlsbad, CA, USA) at 37°C for 48 hours in a 5% CO_2 atmosphere. Then, 100 μL UPBNPs, UPBNPs-MCSNs and CH extracts (prepared by soaking 10mg materials in 1mL ddH$_2$O) were added to each well, respectively. After 1, 3 and 5d, remove the medium from each well and with fresh medium. Incubate in 100 μL α-MEM medium containing 10% Cell Counting Kit-8 (CCK-8, Dojindo Laboratories, Kumamoto, Japan) in dark for 2 h. Absorption was measured with a microplate reader at 450 nm. Untreated cells and α-MEM-only wells served as controls.

TEM Images of Bacteria Treated with the UPBNPs-MCSNs

The morphology of bacteria treated with UPBNPs-MCSNs was characterized by TEM. 10mg UPBNPs-MCSNs were mixed with 500μL of *E. faecalis* suspension (OD600 =1) in BHI (500μL) and co-cultured at 37°C for 24h. Negative control was performed using bacteria. Bacterial cells were collected after washing twice with PBS (Gibco, Grand Island, NY, USA) and fixed with 2.5% glutaraldehyde (Sigma-Aldrich, St. Louis, MO, USA) overnight at 4 ° C. Then they were washed with PBS and postfixed in 1% (wt/vol) osmium tetroxide, dehydrated by ethanol gradient, and finally embedded in resin and section. Ultrathin sections (70 nm) were double-stained with uranyl acetate and lead citrate and observed by TEM (JEOL JEM-1010, JEOL, Japan).

Determination of ROS and LPO Levels in Bacteria

E. faecalis suspension (OD600=1) was co-cultured with UPBNPs and UPBNPs-MCSNs for 24 hours. Bacteria were isolated and suspended again (OD600=1). A suspension of *E. faecalis* was incubated for 20 minutes in darkness at 37°C with 10 μM 2,7-dichlorodihydrofluorescein diacetate (DCFH-DA, Beyotime, China) or C11-BODIPY581/591 (Invitrogen, Carlsbad, CA, USA). Microplate readers (Molecular Devices, Sunnyvale, CA, USA) were used to measure DCF fluorescence intensity (FI) with excitation at 488 nm and emission at 525 nm and oxidized BODIPY FI with excitation at 488 nm and emission at 510 nm. Negative control was performed using BHI, and ROS test positive control was performed using ROSup. Each group was tested 6 times with 3 wells.

Detection of GSH and GSSG Levels in Bacteria

UPBNPs-MCSNs was mixed with 1 mL *E. faecalis* suspension (OD600 =1) make the final concentration 10 mg/mL. BHI was used as the negative control group, GSH/GSSG detection kit (Beyotime, China) was used, and the samples were prepared according to the instructions. Absorption was measured with a microplate reader at 420 nm. Each group was tested 3 times with 6 wells.

Antibiofilm Effect of the UPBNPs-MCSNs in Root Canals

According to the approval of the Ethical Committee Department, the Affiliated Stomatological Hospital of Nanjing Medical University (PJ2020-128-001), mature single mandibular premolars were collected. All clinical investigations have been conducted according to the principles expressed in the Declaration of Helsinki, and informed consent has been obtained from the tissue donors. The exclusion criteria were as follows: incomplete teeth with defects, incomplete root tip development, abnormal development, pulp treatment, pulp calcification, caries or restorations, root fracture or hidden fissure, or jaw disease. The soft tissues of the root surface and dental calculus were removed. The crown and root were cut horizontally at the enamel cementum boundary, leaving the root part. The roots according to standard processes were prepared to F3 size using ProTaper nickel-titanium (NiTi) system (Dentsply Maillefer, Tochigi, Japan). Each canal was rinsed alternately with 17% EDTA solution and 1% NaClO, and the disinfectants were removed with ddH$_2$O and dried.

For sterilization, roots were placed in 3 mL BHI broth and autoclaved sterilization, and cultured with 5 mL *E. faecalis* suspension (OD600=1) at 37°C, 1 week of anaerobic incubation. CH, MCSN and UPBNPs-MCSNs were transported into the root canal and cultured in a sterilization tube at 37°C for 1 week. The root canal was rinsed gently with PBS and dried. 3 samples for each group.

The samples were divided into symmetrical halves. In half of the root, the damage of bacterial biofilm in 3 random regions was observed by FE-SEM (JSM-7900F, JEOL, Japan), and the other half was stained with fluorescent LIVE/ DEAD BacLight Bacterial Viability stain probe (Eugene, OR, USA) to observe the intensity of green fluorescence (live) and red fluorescence (dead) in 3 random regions by CLSM (LSM 710, Carl Zeiss, Germany).

Effects of the UPBNPs-MCSNs Pretreatment on Bacterial Colonization

As mentioned above, the roots were standardized to prepare the root canals and autoclaved. CH, MCSNs and UPBNPs-MCSNs were delivered into the root canal, respectively, and were pretreated at 37 °C for 7 days. Then, gently rinse with PBS to remove the drugs in the root canal. All samples were in 5mL bacterial suspension (OD600=1) at 37 °C for 1 week. Similarly, each root was divided into two symmetrical halves, as in the above method, SEM and CLSM were used to observe the bacterial colonization.

Statistical Analysis

The data were shown as the means ± standard deviation (SD), and were analyzed using one-way analysis of variance and Student's *t*-test. Statistical significance between control and experimental groups was set at $P < 0.05$.

Results

Characterizations of the UPBNPs-MCSNs

SEM and TEM images showed that UPBNPs-MCSNs showed spherical shape with a diameter of about 100 nm (Figure 1A and B). High-resolution TEM (HRTEM) image of UPBNPs-MCSNs showed that the UPBNPs quantum dots (QDs) are uniformly distributed in the channels (red circle) of MCSNs (Figure 1C). Figure 1D showed the HRTEM image of a single UPBNP QD in the UPBNPs-MCSNs, showing obvious UPBNPs lattice fringe, in which the 3.59Å interplanar distances marked with white lines correspond to the (220) plane of the UPBNP phase (Refer to the standard peaks, JCPDS no. 73–0687). EDS analysis showed that UPBNPs-MCSNs were composed of O, Si, C, Ca and Fe elements (Figure 1D). Among them, the Fe element is related to the load of UPBNPs, and the content of 1.35% was close to the theoretical value of 0.90% of Fe in UPBNPs-MCSNs, indicating the complete loading of UPBNPs. The N_2 adsorption-desorption isotherm of MCSNs shows type IV, indicating that they are mesoporous materials with a specific surface area of 104.49 m^2/g, and the diameter of the mesoporous mainly fell in the range of 3–5 nm (Figure 1F). The capillary condensation stage of the N_2 adsorption-desorption isotherm of UPBNPs-MCSNs is significantly slower than that of MCSNs without UPBNPs, indicating that the mesoporous characteristics of the sample are not obvious (Figure 1G). The specific surface area of UPBNPs-MCSNs is 39.91 m^2/g, which is significantly lower than that of MCSNs, indicating that UPBNPs are loaded into the channel of MCSNs.[22]

In order to further evaluate the successful loading of UPBNPs in UPBNPs-MCSNs, the element changes before and after loading UPBNPs and the valence state of Fe after loading was analyzed by XPS, and the chemical bond composition of MCSNs and UPBNPs-MCSNs were analyzed by FT-IR. Figure 1H was the XPS survey scan of MCSNs and UPBNPs-MCSNs. MCSNs contain Si 2p, C 1s, Ca 2p and O 1s characteristic peaks at binding energies of 103, 284, 348 and 532 eV, respectively. On the basis of MCSNs' characteristic peaks, UPBNPs-MCSNs have N 1s and Fe 2p characteristic peaks of 397 and 709 eV. Figure 1I was the high-resolution spectrum of the Fe 2p region of UPBNPs-MCSNs. It deconvolved the four peaks at 708.4, 711.6, 721.4 and 725.4 eV. The bands at 708.4 and 721.4 eV are attributed to Fe $2p_{3/2}$ and Fe $2p_{1/2}$ of Fe^{2+}, respectively, while the peaks at 711.6 and 725.4 eV are attributed respectively to Fe $2p_{3/2}$ and Fe $2p_{1/2}$ of Fe^{3+}.[23] The results show that there are Fe^{2+} and Fe^{3+} in UPBNPs-MCSNs. In FT-IR spectra, MCSNs and UPBNPs-MCSNs had some similar absorption peaks (Figure 1J). At 3416 cm^{-1} is the specific absorption peak of hydroxyl groups (-OH), at 1637 cm^{-1} is the bending vibration peak of water (H-O-H), and at 1076 cm^{-1} is the result of asymmetric stretching vibration of Si-O-Si.[24,25]
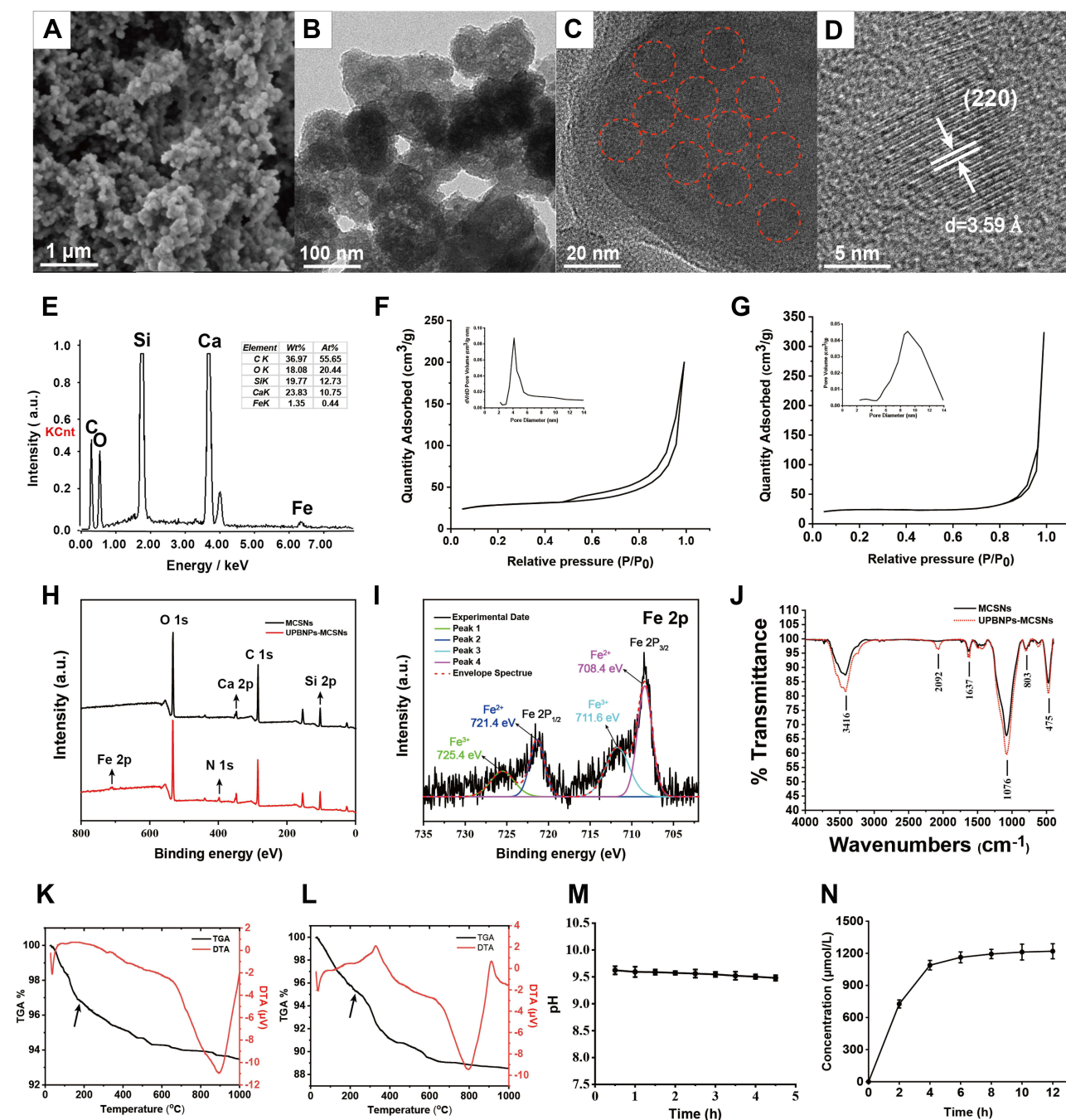
Figure 1 Characterization of the UPBNPs-MCSNs nanocomposites. (**A**) SEM and (**B**) TEM images of the UPBNPs-MCSNs (scale 1μm, 100 nm); (**C**) HRTEM image of the UPBNPs-MCSNs (The red circle shows UPBNPs QDs uniformly distributed in the channel of MCSNs, scale 20 nm); (**D**) HRTEM image of single UPBNP QD in MCSNs (scale 5nm); (**E**) EDS analysis of the UPBNPs-MCSNs; (**F** and **G**) N_2 adsorption-desorption isotherm test and pore size distribution of MCSNs and UPBNPs-MCSNs; (**H**) XPS survey scans of MCSNs and UPBNPs-MCSNs; (**I**) High-resolution XPS spectra of Fe 2p; (**J**) FT-IR spectra of MCSNs and UPBNPs-MCSNs; (**K** and **L**) TGA/DTA diagram of the UPBNPs-MCSNs; (**M**) pH time curve of the UPBNPs-MCSNs; (**N**) Iron ion release curve of the UPBNPs-MCSNs.

The strong absorption peaks at 803 cm^{-1} and 475 cm^{-1} correspond to the symmetric stretching vibration of the Si-O bond.[26] In addition, UPBNPs-MCSNs have a unique absorption peak, showing a C≡N absorption peak at 2092 cm^{-1}, which is characteristic of UPBNPs ($Fe_4[Fe(CN)_6]_3$), implying that UPBNPs are successfully loaded to MCSNs.[27,28]

The thermal stability of MCSNs and UPBNPs-MCSNs in a nitrogen atmosphere at a rate of 10°C/min in the range of room temperature to 1000°C was studied by TGA/DTA (Figure 1K and L). From room temperature to 200°C, the mass loss of MCSNs and UPBNPs-MCSN was 3.32% and 4.68%, respectively, and from 200°C to 1000°C, the mass loss of

MCSNs and UPBNPs-MCSNs was 3.21% and 6.78%, respectively, indicating that MCSNs and UPBNPs-MCSNs had high thermal stability. The DTA curve showed a small endothermic peak at the initial stage, which is due to the removal of water molecules in the material, and a large endothermic peak at around 800 degrees, which is due to thermal degradation.[29,30] In addition, the pH stability and iron release of UPBNPs-MCSNs were examined. The pH values of UPBNPs-MCSNs ranged from 9.7 to 9.5 within 270 mins, which was alkaline and decreased slightly with increasing time (Figure 1M). Iron ions release from UPBNPs-MCSNs was measured within 12h and with time, iron release increased and peaked at 8 hours (Figure 1N).

Antibacterial Activity of the UPBNPs-MCSNs Detected by MTT Assay

The antibacterial activity of *E. faecalis* treated with 1% NaClO was the lowest, only 12% of the initial state, followed by 10 mg/mL UPBNPs-MCSNs group (29.6%), 20 mg/mL USPBNPs-MCSNs (32.0%) and 5 mg/mL UPBNPs-MCSNs group (33.5%). There was no statistical difference between the 2.5 mg/mL UPBNPs-MCSNs group (66.8%) and the negative control group (74.5%) (Figure 2).

Antibacterial Effects of the UPBNPs-MCSNs Detected by CFU Counting Method

All the experimental groups had an antibacterial effect, 10 mg/mL UPBNPs-MCSNs, 1% NaClO, and CH groups showed the best antibacterial activity ($P<0.05$). Importantly, the 10 mg/mL UPBNPs-MCSNs group was significantly superior to the same concentration of UPBNPs and MCSNs alone ($P<0.05$). The antibacterial performances of 5 mg/mL and 2.5 mg/mL UPBNPs-MCSNs groups were weaker than 10mg/mL ($P>0.05$) while still significantly better than negative control group ($P<0.05$) (Figures 3 and 4). Interestingly, metal ion chelator EDTA and antioxidant Vc decreased the antibacterial activity of 10mg/mL UPBNPs-MCSNs (Figure 5) and the antibacterial activity of UPBNPs-MCSNs decreased with the increase of EDTA and Vc concentration ($P<0.05$).

In addition, the antibacterial activity of 10 mg/mL UPBNPs-MCSNs and the same concentration of UPBNPs and MCSNs alone against *S. mutans* was tested by a similar method. We found similar results to *E. faecalis*, with the UPBNPs-MCSNs group significantly superior to the UPBNPs and MCSNs groups alone (Figures 6 and 7).
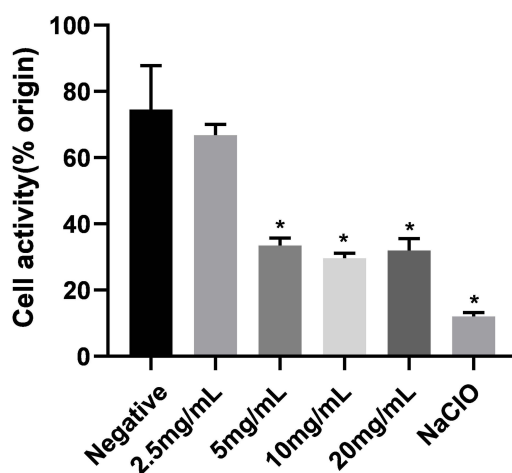

Figure 2 Metabolic activity of *E. faecalis* after treatment. The ratio of the metabolic activity of *E. faecalis* to the initial state of each group after treatment, including the negative control group, UPBNPs-MCSNs groups (2.5 mg/mL, 5 mg/mL, 10 mg/mL and 20 mg/mL), 1% NaClO group. *$P<0.05$ when compared with the negative control group.
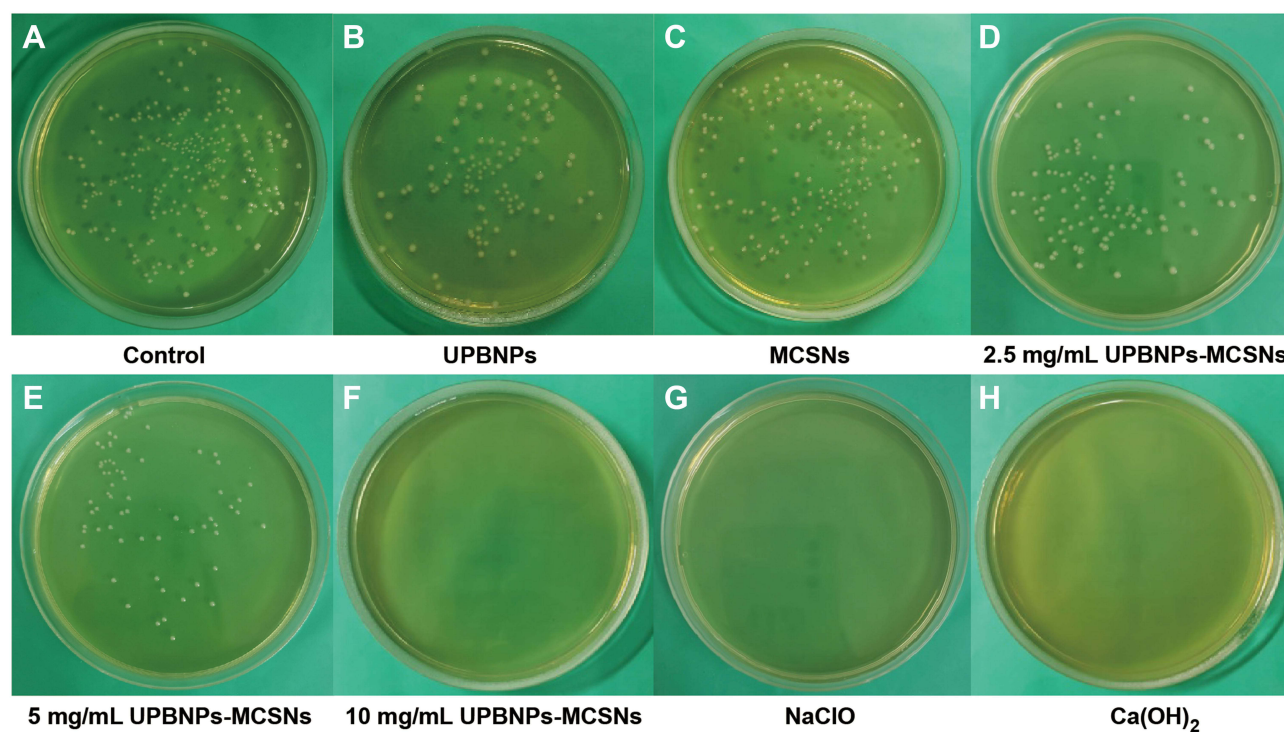
Figure 3 Antibacterial activity of the materials against planktonic *E. faecalis*. (**A**) Negative control group; (**B**) UPBNPs group; (**C**) 10 mg/mL MCSNs group; (**D**)2.5 mg/mL UPBNPs-MCSNs group; (**E**) 5 mg/mL UPBNPs-MCSNs group; (**F**) 10 mg/mL UPBNPs-MCSNs group; (**G**) 1% NaClO group; (**H**) CH group.
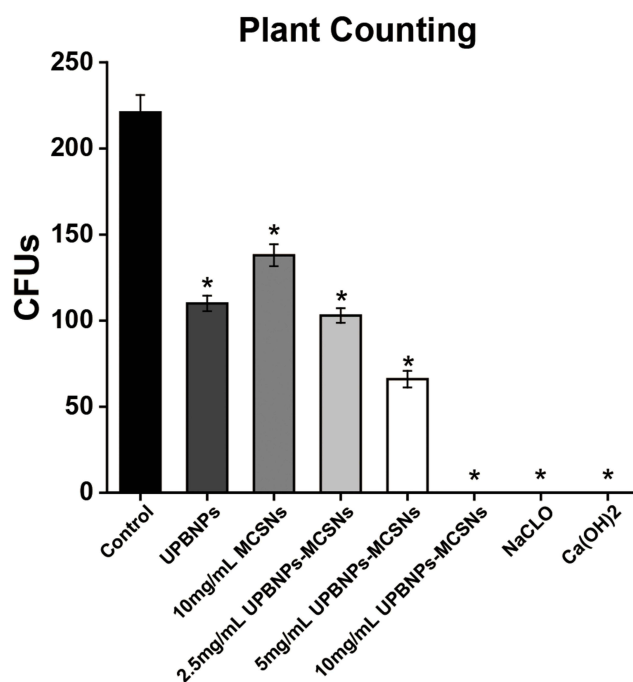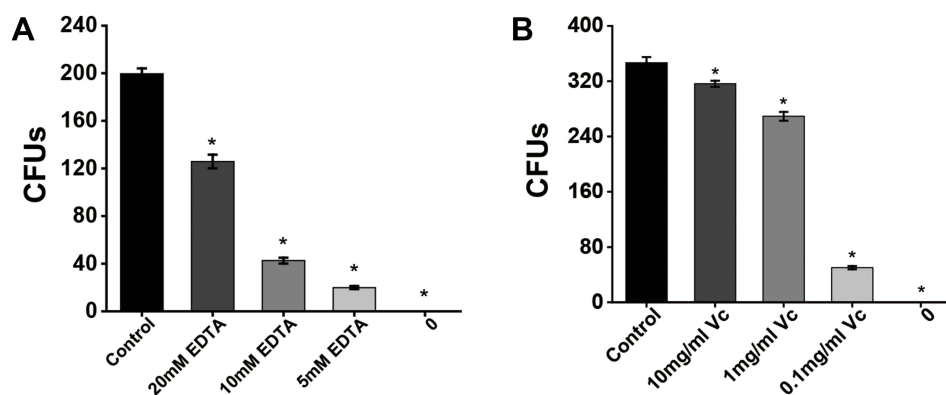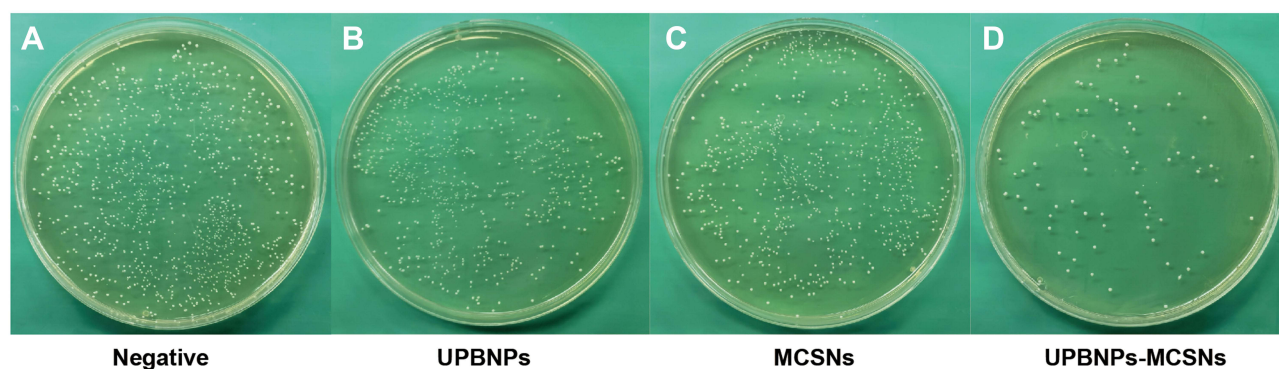

Figure 4 Comparison of antibacterial activity of materials against planktonic *E. faecalis*. Comparison of CFUs counts among all groups, including control group, UPBNPs group, 10 mg/mL MCSNs group, 2.5 mg/mL UPBNPs-MCSNs group, 5 mg/mL UPBNPs-MCSNs group, 10 mg/mL UPBNPs-MCSNs, 1% NaClO group and CH group. *$P<0.05$ when compared with the control group.

Figure 5 Comparison of antibacterial activity of materials added with EDTA and Vc against planktonic *E. faecalis*. (**A**) Comparison of CFU counts among all groups, included control group, 10mg/mL UPBNPs-MCSNs + 20 μM EDTA group, 10mg/mL UPBNPs-MCSNs + 10 μM EDTA group, 10mg/mL UPBNPs-MCSNs + 5 μM EDTA group and UPBNPs-MCSNS group. (**B**) Comparison of CFU counts among all groups, included control group, 10mg/mL UPBNPs-MCSNs + 10 mg/ mL Vc group, 10mg/mL UPBNPs-MCSNs + 1 mg/ mL Vc group and UPBNPs-MCSNS group. * $P<0.05$ when compared with the control group.

Figure 6 Antibacterial activity of the materials against planktonic *S. mutans*. (**A**) Negative control group; (**B**) UPBNPs group; (**C**) 10 mg/mL MCSNs group; (**D**) 10 mg/mL UPBNPs-MCSNs group.

Biosafety of the UPBNPs-MCSNs

After 1 day of incubation, UPBNPs and CH showed significant cytotoxicity to SCAPs ($P<0.05$), however the UPBNPs-MCSNs exhibited no significant cytotoxicity ($P>0.05$) (Figure 8A). The results of incubation for 3 and 5 days were the same as those of 1 day (Figure 8B and C).

Mechanism of the UPBNPs-MCSNs Induced Bacteria Death

TEM images of bacteria showed that *E. faecalis* showed dramatic ultrastructural changes such as plasmolysis after UPBNPs-MCSNs treatment with the control group (Figure 9A and B). The ROS detection results showed that UPBNPs could reduce ROS in bacterial cells ($P<0.05$), while UPBNPs-MCSNs could induce ROS production in bacterial cells ($P<0.05$) (Figure 9C). The LPO detection results showed that UPBNPs-MCSNs induced LPO increased more than 2-fold ($P<0.05$) (Figure 9D). In addition, UPBNPs-MCSNs affected the *E.faecalis* intracellular GSH/GSSG ratio. *E.faecalis* intracellular GSH level decreased ($P<0.05$), GSSG level increased ($P<0.05$), and GSH/GSSG ratio decreased significantly (Figure 9E).

Antibiofilm Effect of the UPBNPs-MCSNs in Root Canals

SEM results exhibited that *E. faecalis* biofilm in the CH and UPBNPs-MCSNs groups showed significant deformation and rupture in contrast to the negative control group (Figure 10A, B and D and a, b, d). However, the biofilm structure of the MCSNs was comparable to that of control group, and the biofilm were more complete, with uniform and dense bacterial biofilm (Figure 10C and c).
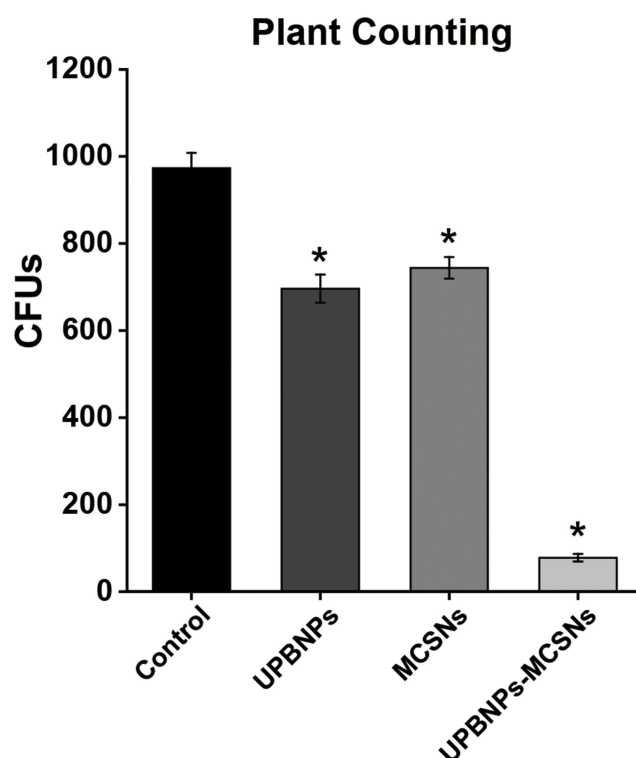
Plant Counting

Figure 7 Comparison of antibacterial activity of materials against planktonic *S. mutans*. Comparison of CFUs counts among all groups, including the control group, UPBNPs group, MCSNs group and UPBNPs-MCSNs. *$P<0.05$ when compared with the control group.
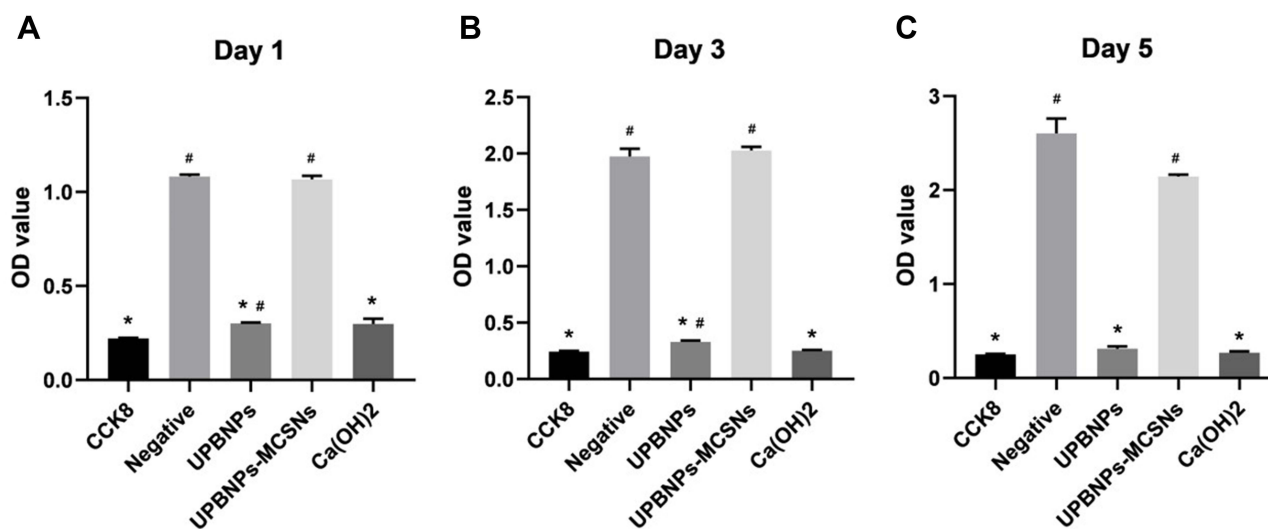

Figure 8 CCK8 test on the SCAPs. (**A**) Culture for 1 day; (**B**) Culture for 3 days; (**C**) Culture for 5 days. The OD values among all groups included the CCK8 group, negative control group, UPBNPs group, UPBNPs-MCSNs group, and CH group. *$P<0.05$ when compared with the negative control group, #$P<0.05$ when compared with the CCK8 group.

CLSM results showed that compared with other groups, the CH group had the largest area of red fluorescence and less obvious green fluorescence (Figure 11B), indicating that the CH group had the most dead bacteria and the least live bacteria. The UPBNPs-MCSNs group showed mostly red fluorescence and a little green fluorescence (Figure 11D), indicating a certain proportion of dead bacteria. However, the negative control group (Figure 11A) and MCSNs group
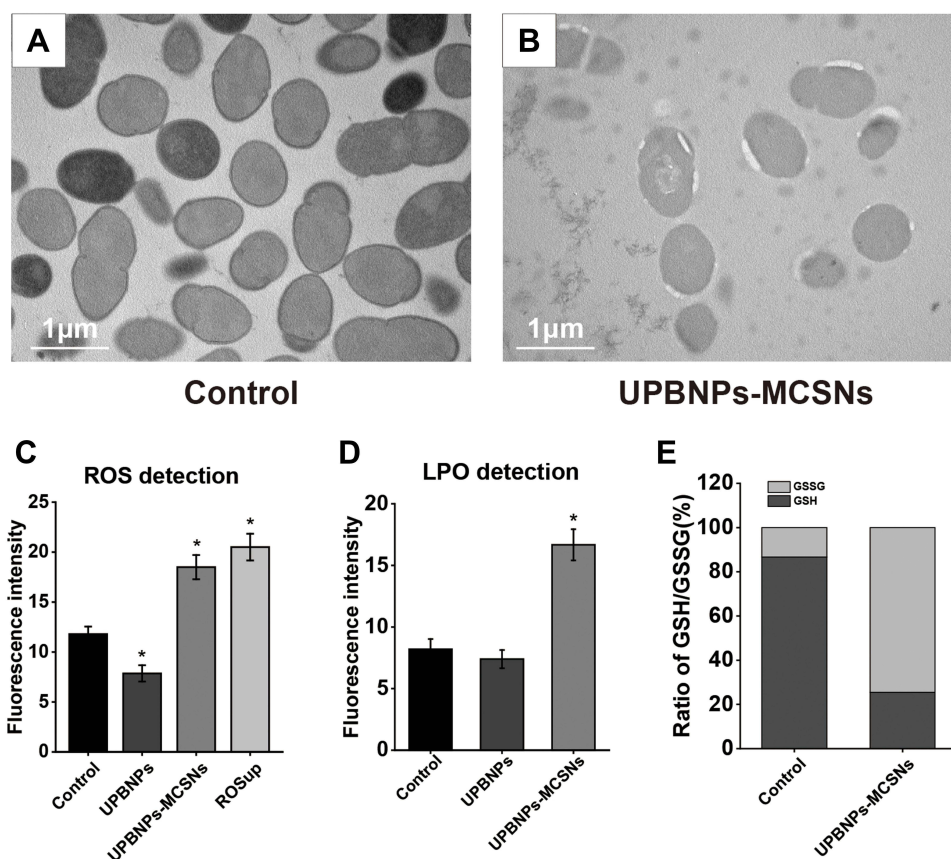
Figure 9 Mechanism of bacterial death induced by UPBNPs-MCSNs. (**A** and **B**) TEM images of *E. faecalis* and *E. faecalis* treated by UPBNPs-MCSNs; (**C**) ROS detection of *E. faecalis* treated with materials, including the control group, UPBNPs group, UPBNPs-MCSNs group, and ROSup group. *$P<0.05$ when compared with the control group; (**D**) PLO detection of *E. faecalis* treated with materials, including the control group, UPBNPs group and UPBNPs-MCSNs group. *$P<0.05$ when compared with the control group; (**E**) GSH balance in *E. faecalis* treated by UPBNPs-MCSNs, including the control group and UPBNPs-MCSNs group.

(Figure 11C) showed more areas of green fluorescence, indicating the biofilm contained a high proportion of viable bacteria.

Effects of UPBNPs-MCSNs Pretreatment on Bacterial Colonization

SEM results displayed a great many *E. faecalis* colonization of negative control and CH groups (Figure 12A, B and a, b). Furthermore, the colonization of *E. faecalis* was more intensive after pretreatment with CH than in the negative control group. Few bacteria were observed in the MCSNs and UPBNPs-MCSNs, among which UPBNPs-MCSNs had the least bacterial attachment (Figure 12C, D and c, d).

CLSM results showed dense and strong green fluorescence of negative control and CH groups (Figure 13A and B), suggesting that more *E. faecalis* was colonized on the canal walls. However, after pretreatment with MCSNs and UPBNPs-MCSNs, the green fluorescence on the root canal walls was very weak, which was the least in the UPBNPs-MCSNs group, indicating that *E. faecalis* survived and attached less in the root canal (Figure 13C and D).

Discussion

Antibiotic resistance is a significant threat to human health, making it increasingly difficult for the conventional treatment of bacterial infections. Unlike antibiotics, microbes generally do not develop resistance to nanomaterials.[31] In terms of dental endodontics, the development and research of nanomaterials are mainly concentrated on improving antibacterial activity.[32] To solve the problem of bacterial resistance to antibiotics, some scholars have developed submicron or nanoscale materials, such as silver nanoparticles and chitosan nanoparticles, which are carried with antibacterial agents and introduce antibacterial activity into irregular root canals.[33–35] In addition, many surface modification technologies of materials focus on applying
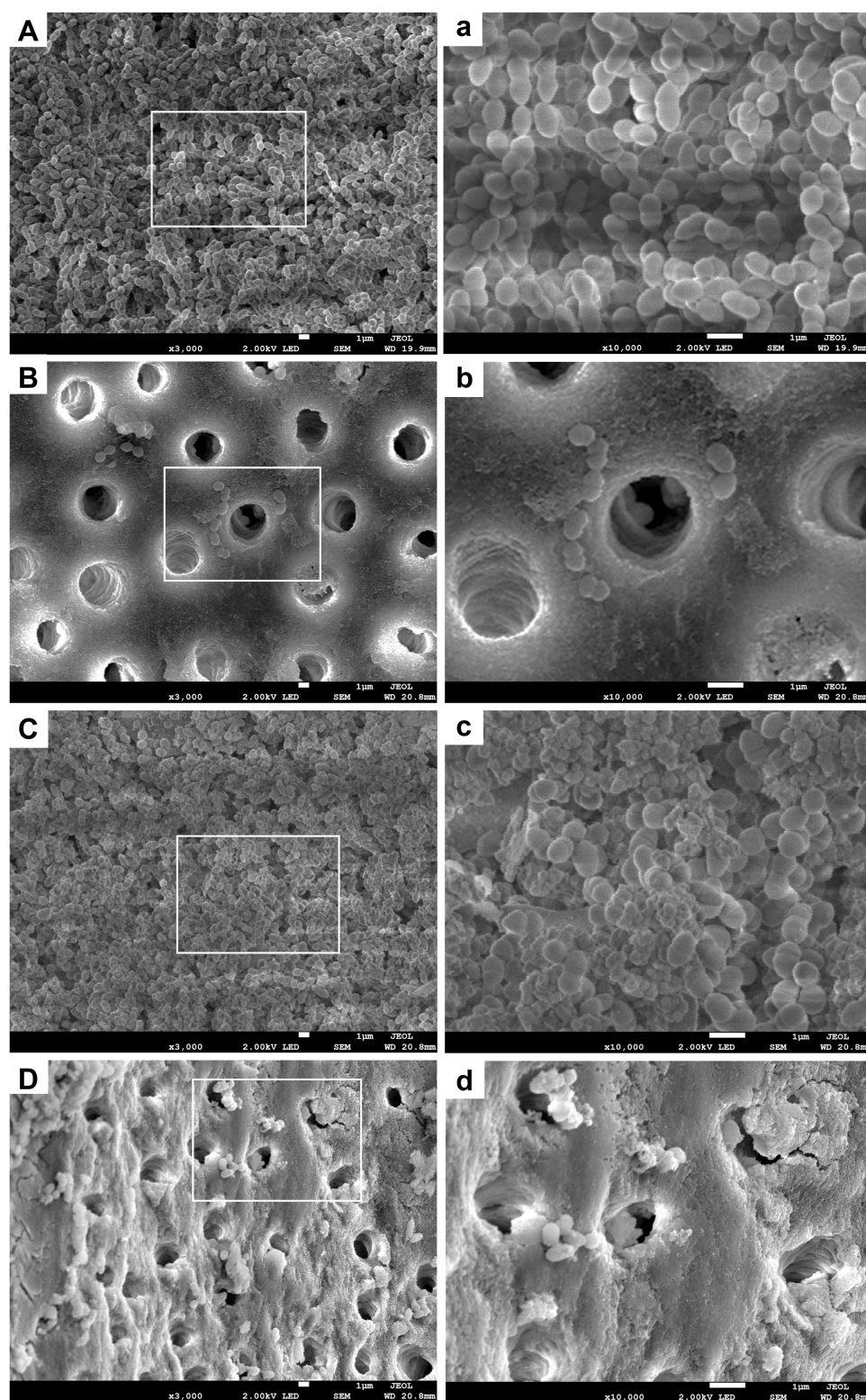
Figure 10 SEM results of *E. faecalis* biofilm in root canals treated with materials (capital letters: ×3000 magnification; small letters: ×10,000 magnification). (A and a) negative control group; (B and b) CH group; (C and c) MCSNs group; (D and d) UPBNPs-MCSNs group.
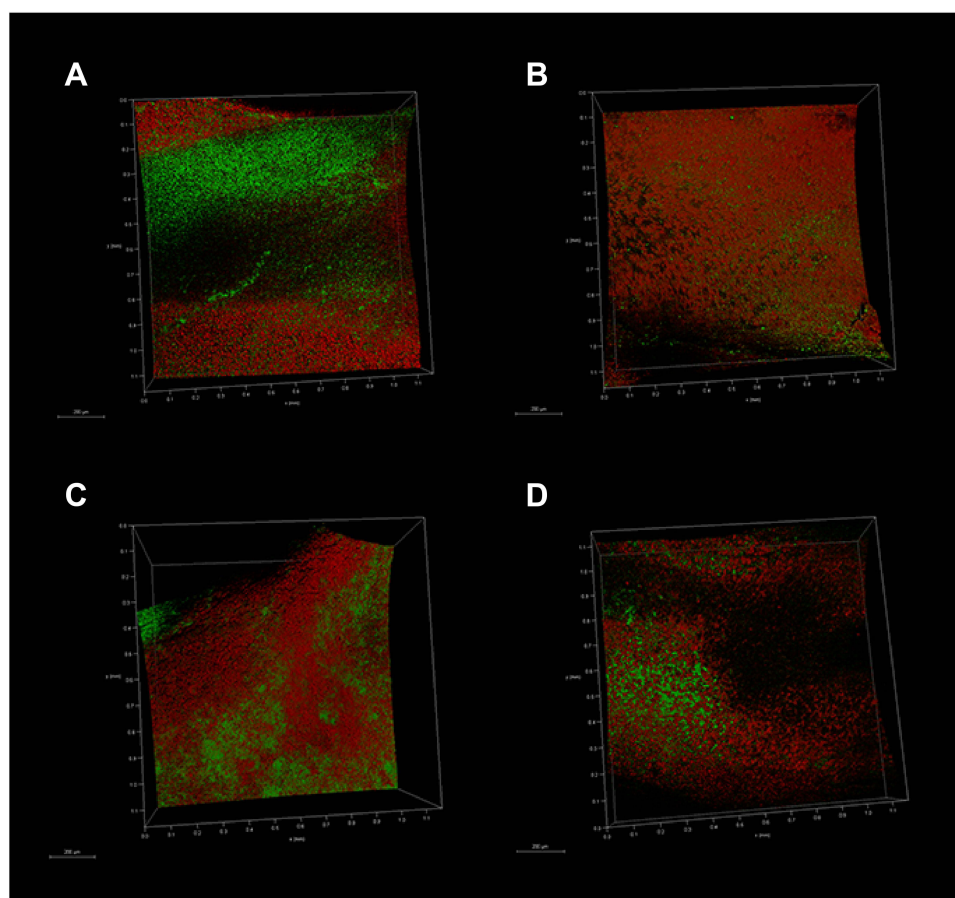
Figure 11 CLSM 3-dimensional reconstructions of *E. faecalis* biofilm on root canal walls after materials treatment. (**A**) Negative control group; (**B**) CH group; (**C**) MCSNs group; (**D**) UPBNPs-MCSNs group.

anti-biological pollution and anti-adhesion surface coatings and use the concept of surface chemistry to change the surface functionality and improve the ability of the surface to resist bacteria.[36] The UPBNPs-MCSNs synthesized in this study have characteristic nano size, forming a slightly alkaline environment and continuously releasing iron ions.

CH is the commonly used root canal disinfection drug in endodontics. Because of the strong alkaline, which makes bacterial cell membrane rupture, protein denaturation, and DNA damage.[37] However, the high pH of CH is easy to be adapted by bacteria and cannot achieve the effect of long-term sterilization.[38] Long-term CH sealing can reduce the mechanical properties of dentin.[39] NaClO is the commonly used root canal rinse in root canal therapy but has the disadvantages of pungent odor, high cytotoxicity and occasional allergic reaction, and its antibacterial activity is easily affected by pH value and temperature.[40] It can also cause cell damage to normal tissues around the apical and affect the repair process.[41] Our previous studies have shown that MCSNs release Ca^{2+} and SiO_4^{4-} in liquid to form a weakly alkaline microenvironment, and its nanometer size will interfere with bacterial metabolism, but the antibacterial activity of MCSNs is still weak.[42] UPBNPs-MCSNs showed excellent antibacterial ability, and the antibacterial activity of UPBNPs-MCSNs against *E. faecalis* increased with concentration when the concentration was lower than 10 mg/mL. However, the MTT test showed that the antibacterial activity of UPBNPs-MCSNs at 20 mg/mL was not better than UPBNPs-MCSNs at 10 mg/mL. It is speculated that this might be related to the excessive concentration of nanomaterials, resulting in the saturation of effective ions in suspension or the influence of high concentration on ion release. In addition, CCK8 results showed that UPBNPs-MCSNs had a selective killing effect on cells and showed good biocompatibility to SCAPs while maintaining its strong antibacterial effect.

Recent studies have shown that disruption of ROS dynamic balance and lipid peroxidation can lead to cell ferroptosis.[43] In this study, we demonstrate for the first time that iron and ROS-dependent ferroptosis are involved in
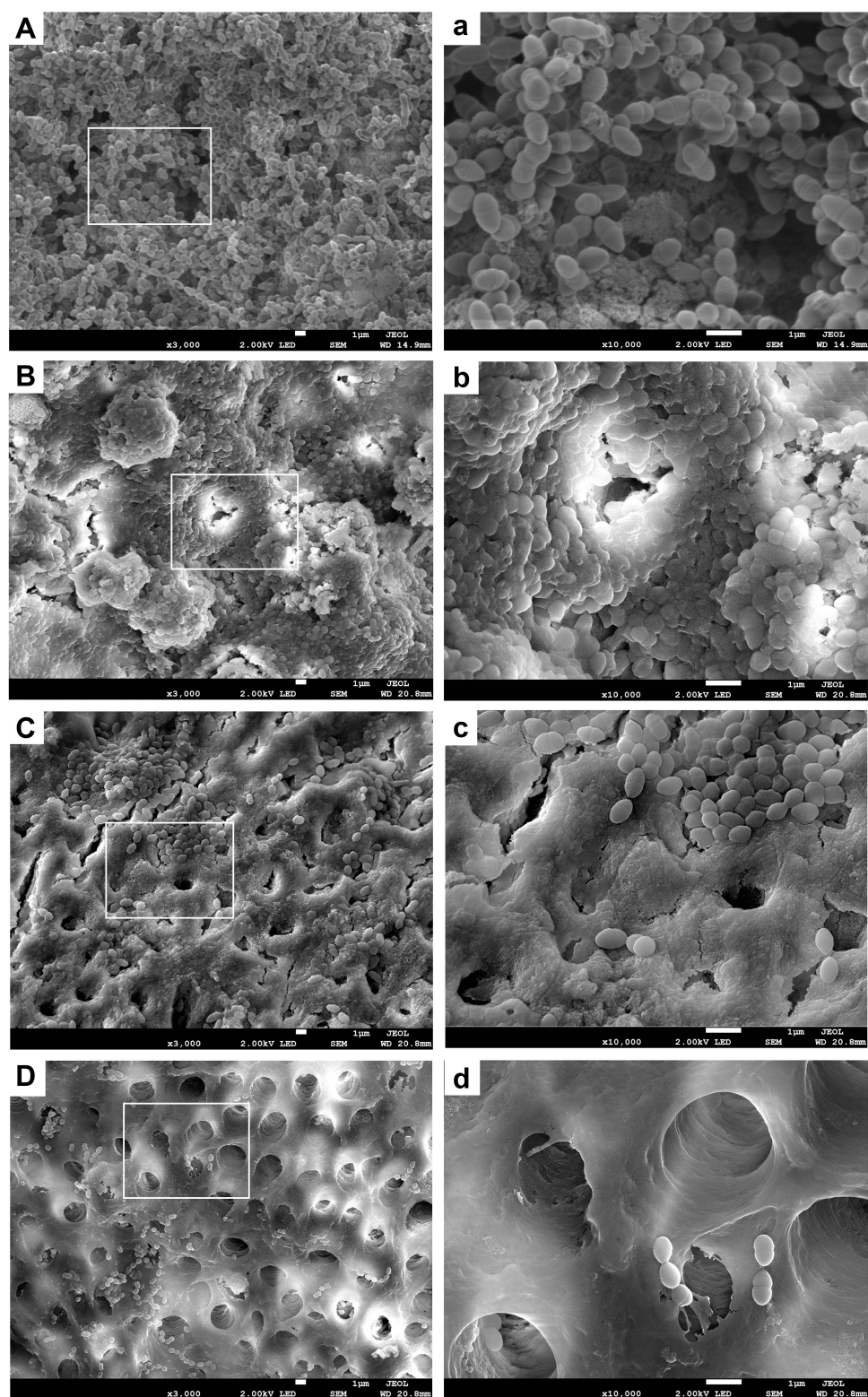
Figure 12 SEM results of colonization of *E. faecalis* in the pretreated root canal (capital letters: × 3000 magnification; small letters: ×10,000 magnification). (**A** and a) negative control group; (**B** and b) CH group; (**C** and c) MCSNs group; (**D** and d) UPBNPs-MCSNs group.
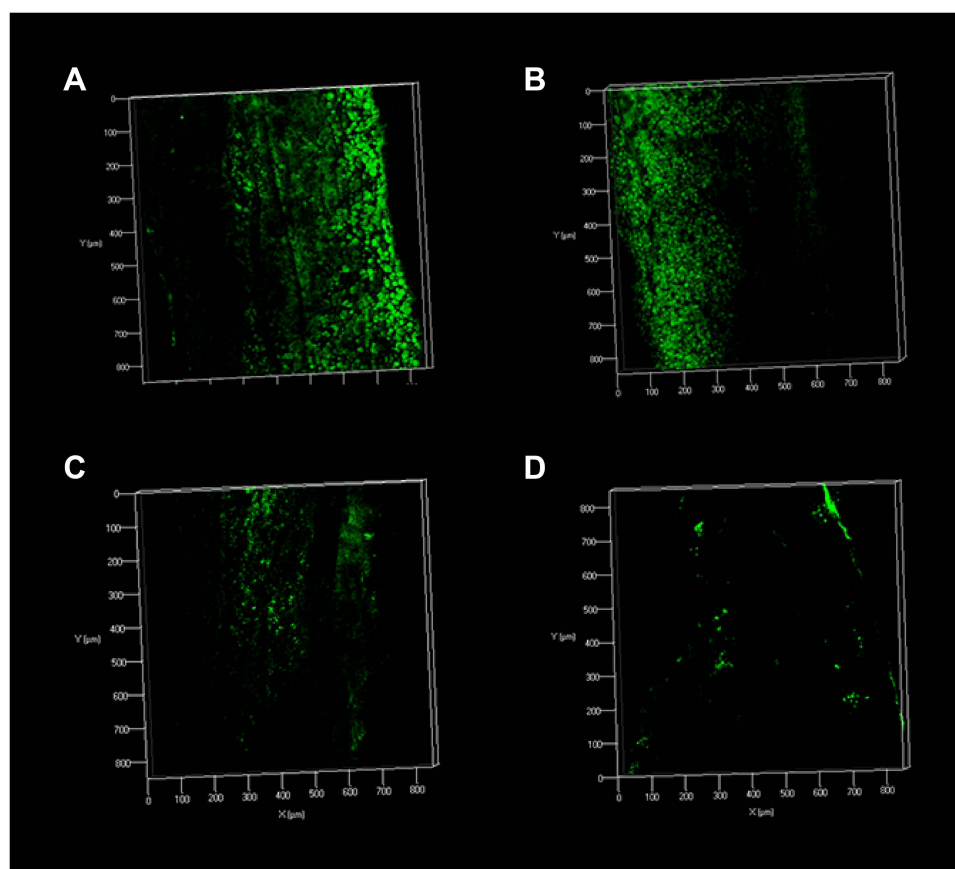
Figure 13 CLSM 3-dimensional reconstruction images of *E. faecalis* colonization on the pretreated root canal walls. (**A**) Negative control group; (**B**) CH group; (**C**) MCSNs group; (**D**) UPBNPs-MCSNs group.

E. faecalis death. Single iron oxide nanomaterials have weak antibacterial activity under physiological conditions, while multi-functionalized iron oxide nanoparticles were significantly enhanced in antibacterial activity, resulting in the ferroptosis-like death of bacteria.[19] The results of this study are also consistent with the recent developments of bacterial death caused by other types of iron nanomaterials. For example, Li et al found that FePPOP$_{BFPB}$ containing iron showed excellent peroxide-like activity, when combined with near-infrared light absorption, it can effectively catalyze H_2O_2 of bio-related concentration to produce a large amount of hydroxyl radicals (·OH) through the Fenton reaction, FePPOP$_{BFPB}$ has an obvious bactericidal effect on *Staphylococcus aureus* under near-infrared radiation.[44] Bukhari et al used biomimetic iron oxide nanoparticles to enhance the activity of H_2O_2, and the combination of the two drugs can enhance the effect of root canal disinfection and improve the antibacterial effect of *E. faecalis*.[45] Excessive exogenous or endogenous ROS will cause a series of damage to the body, and there are also various antioxidant substances with a strong reductive ability to regulate ROS.[46] Iron-based nanomaterials can produce ROS and cause oxidative stress, resulting in permanent damage to DNA, lipids, and proteins in cells, among which lipids are the main targets of oxidative damage.[47] Due to the widespread presence of polyunsaturated fatty acids on cell membranes, the reaction of these oxidized free radicals with lipids to generate LPO results in decreased cell membrane fluidity to change membrane properties and destroy membrane proteins.[48] The bases and ribose in DNA are attacked by ROS, leading to the breakage of DNA double-stranded structure and abnormal replication, making mutations more likely.[49]

Therefore, it is inferred that the excellent antibacterial activity of UPBNPs-MCSNs may be related to the induction of bacteria to produce more ROS and LPO. UPBNPs-MCSNs have been detected to release Fe ions. Therefore, under the action of Fe ions (especially Fe^{2+}), they increase the generation of ROS through the Fenton reaction. However, UPBNPs can reduce ROS production, which is consistent with the study of Zhao et al.[50] The possible reason is that UPBNPs alone does not produce ·OH through the Fenton reaction.[51] At the same time, the increased ROS consumed GSH in bacteria, and the

antioxidant system was out of balanced. Excessive ROS induces the highly expressed unsaturated fatty acids on the bacterial cell membrane to generate LPO, which damages the membrane, protein and nucleic acid of bacteria and leads to the plasmolysis and death of bacteria (Figure 14). However, antioxidant Vc and metal ions chelator EDTA inhibited the antibacterial activity of UPBNPs-MCSNs on *E. faecilis*. These results suggest that UPBNPs-MCSNs promote bacterial death by regulating the antioxidant system, which is manifested as the ROS/GSH pathway of ferroptosis-like death.

In this study, the antibacterial activity of MCSNs on biofilm was mediocre and much lower than CH, which was consistent with previous research results.[11] UPBNPs-MCSNs showed a similar antibiofilm effect to CH, indicating that they could effectively destroy the structure of biofilm and kill *E. faecalis*. Moreover, affinity to dentin is an essential feature of the excellent root canal disinfectant, which can still have the antibacterial effect after removal for a period of time, and is of great value for removing residual bacteria and preventing root canal reinfection after root canal preparation and filling.[52] Previous studies have shown that small-size nanomaterials have better permeability than large-size materials,[53] and their mesoporous structure can carry metal ions, antibiotics, and other drugs, which can be released continuously to produce effects.[54] Fan et al found that CH had a poor affinity for dentin surface and could not
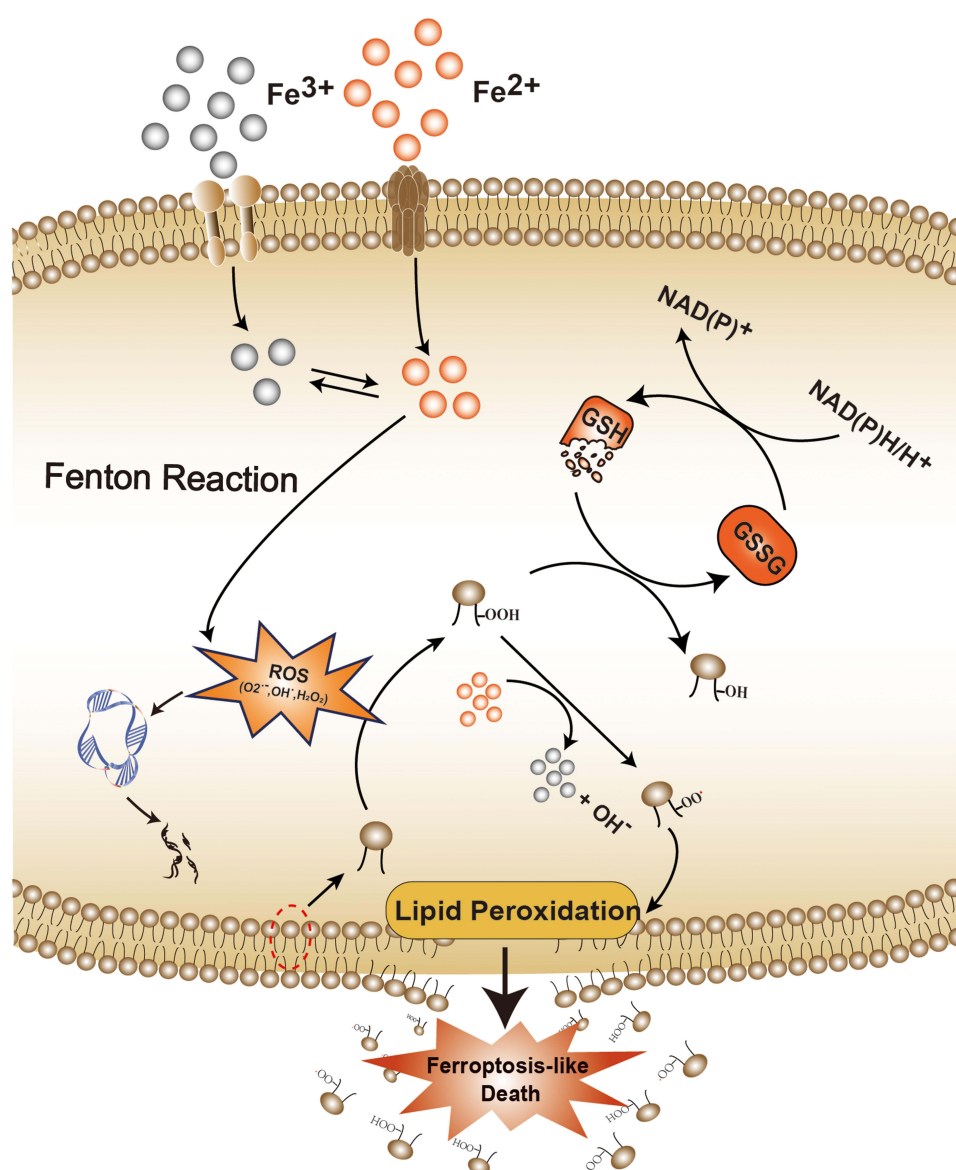

Figure 14 The antibacterial mechanism schematic of UPBNPs-MCSNs.

continue to exert an antibacterial effect after removal.[55] Leng et al exhibited that CH had no affinity to the root canal surface and even enriched *E. faecalis*, the reason probable that the strongly alkaline environment generated by CH denatures organic components in dentin and enhances the attachment and colonization of *E. faecalis*.[11] The results of this research were in agreement with the above views. CH pretreatment group could not produce sustained antibacterial performance and formed complete and dense biofilm on the root canal walls, which was more likely to induce *E. faecalis* colonization than the negative group. MCSNs ability to promote apatite mineralization makes it adsorb to the root canal walls and resist *E. faecalis* adhesion and proliferation to a certain extent.

Conclusion

Overall, our findings exhibit that UPBNPs-MCSNs have high antibacterial performance against bacteria and its biofilm by mediating the redox pathway ROS/GSH in bacteria, which is a like classic pathway to ferroptosis, without significant cytotoxicity to normal cells. In addition, the root canal wall pretreated with UPBNPs-MCSNs can effectively prevent the attachment of *E. faecalis*, which is stronger than the commonly used clinical root canal disinfectant CH. Therefore, ferroptosis may become a potential strategy for the treatment of *E. faecalis* infection in root canals, and UPBNPs-MCSNs are expected to develop into a safe and effective novel root canal disinfectant.

Acknowledgments

Disclosure

The authors report no conflicts of interest in this study.

References

1. Hussein H, Kishen A. Local immunomodulatory effects of intracanal medications in apical periodontitis. *J Endod*. 2022;S0099-2399(22):8.
2. Zhang C, Yang Z, Hou B. Diverse bacterial profile in extraradicular biofilms and periradicular lesions associated with persistent apical periodontitis. *Int Endod J*. 2021;54:1425–1433. doi:10.1111/iej.13512
3. Y-L N, Mann V, Gulabivala K. Tooth survival following non-surgical root canal treatment: a systematic review of the literature. *Int Endod J*. 2010;43:171–189. doi:10.1111/j.1365-2591.2009.01671.x
4. Ng Y-L, Mann V, Gulabivala K. Outcome of secondary root canal treatment: a systematic review of the literature. *Int Endod J*. 2008;41 (12):1026–1046. doi:10.1111/j.1365-2591.2008.01484.x
5. Segura-Egea J, D. C, Martín-González J, et al. Impact of systemic health on treatment outcomes in endodontics. *Int Endod J*. 2022. doi:10.1111/iej.13789
6. Thienngern P, Panichuttra A, Ratisoontorn C, Aumnate C, Matangkasombut O. Efficacy of chitosan paste as intracanal medication against Enterococcus faecalis and Candida albicans biofilm compared with calcium hydroxide in an in vitro root canal infection model. *BMC Oral Health*. 2022;22(1):354. doi:10.1186/s12903-022-02385-x
7. Barbosa-Ribeiro M, Arruda-Vasconcelos R, Louzada LM, Dos Santos DG, Andreote FD, Gomes BPFA. Microbiological analysis of endodontically treated teeth with apical periodontitis before and after endodontic retreatment. *Clin Oral Investig*. 2021;25(4):2017–2027. doi:10.1007/s00784-020-03510-2
8. Hu T, Lei L, Zhou XD. [Research progress in pathogenesis and control of Enterococcus faecalis with persistent infection in root canals]. *Zhonghua Kou Qiang Yi Xue Za Zhi = Zhonghua Kouqiang Yixue Zazhi = Chinese Journal of Stomatology*. 2022;57(1):10–15. doi:10.3760/cma.j.cn112144-20210929-00446
9. Wu C, Chang J, Fan W. Bioactive mesoporous calcium–silicate nanoparticles with excellent mineralization ability, osteostimulation, drug-delivery and antibacterial properties for filling apex roots of teeth. *J Mater Chem*. 2012;22(33):16801–16809. doi:10.1039/c2jm33387b
10. Sun Q, Duan M, Fan W, Fan B. Ca-Si mesoporous nanoparticles with the optimal Ag-Zn ratio inhibit the *Enterococcus faecalis* infection of teeth through dentinal tubule infiltration: an in vitro and in vivo study. *J Mater Chem B*. 2021;9(9):2200–2211. doi:10.1039/D0TB02704A
11. Leng D, Li Y, Zhu J, et al. The Antibiofilm Activity and Mechanism of Nanosilver- and Nanozinc-Incorporated Mesoporous Calcium-Silicate Nanoparticles. *Int J Nanomedicine*. 2020;15:3921–3936. doi:10.2147/IJN.S244686
12. Fan W, Wu D, Tay FR, Ma T, Wu Y, Fan B. Effects of adsorbed and template nanosilver in mesoporous calcium-silicate nanoparticles on inhibition of bacteria colonization of dentin. *Int J Nanomedicine*. 2014;9:5217–5230. doi:10.2147/IJN.S73144
13. Zhu J, Liang R, Sun C, Xie L, Wang J. Effects of nanosilver and nanozinc incorporated mesoporous calcium-silicate nanoparticles on the mechanical properties of dentin. *PLoS One*. 2017;12(8):e0182583. doi:10.1371/journal.pone.0182583
14. Xiao L, Yanbin C, Jiong L, et al. Folic acid-modified Prussian blue/polydopamine nanoparticles as an MRI agent for use in targeted chemo/photothermal therapy. *Biomater Sci*. 2019;7:2996–3006. doi:10.1039/C9BM00276F
15. Antònia BM, Joan E. Prussian blue nanoparticles: synthesis, surface modification, and biomedical applications. *Drug Discov Today*. 2020;25:1431–1443. doi:10.1016/j.drudis.2020.05.014

16. Qin Z, Li Y, Gu N. Progress in applications of Prussian blue nanoparticles in biomedicine. *Adv Healthc Mater*. 2018;7(20):e1800347. doi:10.1002/adhm.201800347

17. Qin Z, Chen B, Mao Y, et al. Achieving ultrasmall Prussian blue nanoparticles as high-performance biomedical agents with multifunctions. *ACS Appl Mater Interfaces*. 2020;12(51):57382–57390. doi:10.1021/acsami.0c18357

18. Li J, Liu X, Tan L, et al. Prussian blue enhances photothermal clearance of *Staphylococcus aureus* and promotes tissue repair in infected wounds. *Nat Commun*. 2019;10(1):4490. doi:10.1038/s41467-019-12429-6

19. Shen X, Ma R, Huang Y, Chen L. Nano-decocted ferrous polysulfide coordinates ferroptosis-like death in bacteria for anti-infection therapy. *Nano Today*. 2020;35:100981. doi:10.1016/j.nantod.2020.100981

20. Zhang K, Wu J, Zhao X, et al. Prussian Blue/Calcium Peroxide Nanocomposites-Mediated Tumor Cell Iron Mineralization for Treatment of Experimental Lung Adenocarcinoma. *ACS nano*. 2021;15(12):19838–19852. doi:10.1021/acsnano.1c07308

21. Dixon SJ, Lemberg KM, Lamprecht MR, et al. Ferroptosis: an iron-dependent form of nonapoptotic cell death. *Cell*. 2012;149(5):1060–1072. doi:10.1016/j.cell.2012.03.042

22. Lun Z, Shuiqing G, Yinghua X, et al. Musca domestica Colon tissue-accumulating mesoporous carbon nanoparticles loaded with cecropin for ulcerative colitis therapy. *Theranostics*. 2021;11:3417–3438. doi:10.7150/thno.53105

23. Yamashita T, Hayes P. Analysis of XPS spectra of Fe 2+ and Fe 3+ ions in oxide materials. *Appl Surf Sci*. 2008;254(8):2441–2449. doi:10.1016/j.apsusc.2007.09.063

24. Zhang S, Lu Y, Ye X. Catalytic behavior of carbonic anhydrase enzyme immobilized onto nonporous silica nanoparticles for enhancing CO_2 absorption into a carbonate solution. *Int J Greenhouse Gas Control*. 2013;13:17–25. doi:10.1016/j.ijggc.2012.12.010

25. Hosseinipour SL, Khiabani MS, Hamishehkar H, Salehi R. Enhanced stability and catalytic activity of immobilized alpha-amylase on modified Fe3O4 nanoparticles for potential application in food industries. *J Nanoparticle Res*. 2015;17(9):2548.

26. Limón-Pacheco JH, Jiménez-Barrios N, Déciga-Alcaraz A, et al. Astrocytes Are More Vulnerable than Neurons to Silicon Dioxide Nanoparticle Toxicity in Vitro. *Toxics*. 2020;8(3):548. doi:10.3390/toxics8030051

27. Nilchi A, Saberi R, Moradi M, et al. Adsorption of cesium on copper hexacyanoferrate-PAN composite ion exchanger from aqueous solution. *Chem Eng J*. 2011;172(1):572–580. doi:10.1016/j.cej.2011.06.011

28. Peng X, Zheng J, Wang J, et al. Synthesis of hollow mesoporous silica spheres functionalized with copper ferrocyanide and its application for Cs removal. *Environ Sci Pollut Res Int*. 2022;29(35):53509–53521. doi:10.1007/s11356-022-19659-0

29. Zaidi R, Khan SU, Farooqi IH, Azam A. Investigation of kinetics and adsorption isotherm for fluoride removal from aqueous solutions using mesoporous cerium-aluminum binary oxide nanomaterials. *RSC Adv*. 2021;11(46):28744–28760. doi:10.1039/D1RA00598G

30. Hasanpour Galehban M, Zeynizadeh B, Mousavi H. Diverse and efficient catalytic applications of new cockscomb flower-like Fe3O4@SiO2@KCC-1@MPTMS@CuII mesoporous nanocomposite in the environmentally benign reduction and reductive acetylation of nitroarenes and one-pot synthesis of some coumarin compounds. *RSC Adv*. 2022;12(18):11164–11189. doi:10.1039/D1RA08763K

31. Rai MK, Deshmukh SD, Ingle AP, Gade AK. Silver nanoparticles: the powerful nanoweapon against multidrug-resistant bacteria. *J Appl Microbiol*. 2012;112(5):841–852. doi:10.1111/j.1365-2672.2012.05253.x

32. Shrestha A, Kishen A. Antibacterial Nanoparticles in Endodontics: a Review. *J Endod*. 2016;42(10):1417–1426. doi:10.1016/j.joen.2016.05.021

33. Zand V, Mokhtari H, Hasani A, Jabbari G. Comparison of the Penetration Depth of Conventional and Nano-Particle Calcium Hydroxide into Dentinal Tubules. *Iran Endod J*. 2017;12(3):366–370. doi:10.22037/iej.v12i3.16421

34. Del Carpio-Perochena A, Kishen A, Shrestha A, Bramante CM. Antibacterial Properties Associated with Chitosan Nanoparticle Treatment on Root Dentin and 2 Types of Endodontic Sealers. *J Endod*. 2015;41(8):1353–1358. doi:10.1016/j.joen.2015.03.020

35. Wu D, Fan W, Kishen A, Gutmann JL, Fan B. Evaluation of the antibacterial efficacy of silver nanoparticles against *Enterococcus faecalis* biofilm. *J Endod*. 2014;40(2):285–290. doi:10.1016/j.joen.2013.08.022

36. Linklater DP, Baulin VA, Juodkazis S, Crawford RJ, Stoodley P, Ivanova EP. Mechano-bactericidal actions of nanostructured surfaces. *Nat Rev Microbiol*. 2021;19(1):8–22. doi:10.1038/s41579-020-0414-z

37. Gluskin AH, Lai G, Peters CI, Peters OA. The double-edged sword of calcium hydroxide in endodontics: precautions and preventive strategies for extrusion injuries into neurovascular anatomy. *J Am Dent Assoc*. 2020;151(5):317–326. doi:10.1016/j.adaj.2020.01.026

38. Gokalp C, Serhan OC, Duygu YH. Evaluation of Antibacterial and Antifungal Effects of Calcium Hydroxide Mixed with Two Different Essential Oils. *J Molecules*. 2022;27:215.

39. Yassen Ghaeth H, Chu Tien-Min G, Eckert G, Platt JA. Effect of Medicaments Used in Endodontic Regeneration Technique on the Chemical Structure of Human Immature Radicular Dentin: an In Vitro Study. *J Endod*. 2013;39(2):269–273. doi:10.1016/j.joen.2012.09.020

40. Coaguila-Llerena H, Barbieri I, Tanomaru-Filho M, et al. Physicochemical properties, cytotoxicity and penetration into dentinal tubules of sodium hypochlorite with and without surfactants. *Restor Dent Endod*. 2020;1(4):487.

41. Faria G, Viola KS, Coaguila-Llerena H, et al. Penetration of sodium hypochlorite into root canal dentine: effect of surfactants, gel form and passive ultrasonic irrigation. *Int Endod J*. 2019;52(3):385–392. doi:10.1111/iej.13015

42. Wu D, Fan W, Kishen A, Gutmann JL, Fan B. Evaluation of the antibacterial efficacy of silver nanoparticles against *Enterococcus faecalis* biofilm. *J Endod*. 2014;40(2):285–290.

43. Qi X, Zhang Y, Guo H, Hai Y, Luo Y, Yue T. Mechanism and intervention measures of iron side effects on the intestine. *Crit Rev Food Sci Nutr*. 2020;60(12):2113–2125. doi:10.1080/10408398.2019.1630599

44. Li D, Fang Y, Zhang ZX. Bacterial Detection and Elimination Using a Dual-Functional Porphyrin-Based Porous Organic Polymer with Peroxidase-Like and High Near-Infrared-Light-Enhanced Antibacterial Activity. *ACS Appl Mater Interfaces*. 2020;12(8):8989–8999. doi:10.1021/acsami.9b20102

45. Bukhari S, Kim D, Liu Y, Karabucak B, Koo H. Novel endodontic disinfection approach using catalytic nanoparticles. *J Endod*. 2018;44(5):806–812. doi:10.1016/j.joen.2017.12.003

46. Finkel T, Holbrook NJ. Oxidants, oxidative stress and the biology of ageing. *Nature*. 2000;408(6809):239–247. doi:10.1038/35041687

47. Park S-C, Kim N-H, Yang W, Nah J-W, Jang M-K, Lee D. Polymeric micellar nanoplatforms for Fenton reaction as a new class of antibacterial agents. *J Control Release*. 2016;221:37–47. doi:10.1016/j.jconrel.2015.11.027

48. Cabiscol E, Tamarit J, Ros J. Oxidative stress in bacteria and protein damage by reactive oxygen species. *Int Microbiol*. 2010;3(1):3–8.

49. DeFedericis H-C, Patrzyc HB, Rajecki MJ, et al. Singlet oxygen-induced DNA damage. *Radiat Res*. 2006;165(4):445–451. doi:10.1667/RR3533.1

50. Zhao J, Cai X, Gao W, et al. Prussian Blue Nanozyme with Multienzyme Activity Reduces Colitis in Mice. *ACS Appl Mater Interfaces*. 2018;10 (31):26108–26117. doi:10.1021/acsami.8b10345

51. Zhang W, Hu S, Yin -J-J, et al. Prussian Blue Nanoparticles as Multienzyme Mimetics and Reactive Oxygen Species Scavengers. *J Am Chem Soc*. 2016;138(18):5860–5865. doi:10.1021/jacs.5b12070

52. Fan W, Wu Y, Ma T, Li Y, Fan B. Substantivity of Ag–Ca–Si mesoporous nanoparticles on dentin and its ability to inhibit *Enterococcus faecalis*. *J Mater Sci Mater Med*. 2016;27(1):16. doi:10.1007/s10856-015-5633-x

53. Moritz M, Geszke-Moritz M. Mesoporous materials as multifunctional tools in biosciences: principles and applications. *Mater Sci Eng C Mater Biol Appl*. 2015;49:114–151. doi:10.1016/j.msec.2014.12.079

54. Fan B, Fan W, Wu D, Tay F, Ma T, Wu Y. Effects of adsorbed and templated nanosilver in mesoporous calcium-silicate nanoparticles on inhibition of bacteria colonization of dentin. *Int J Nanomedicine*. 2014;9:5217–5230.

55. Fan W, Wu Y, Ma T, Li Y, Fan B. Substantivity of Ag–Ca–Si mesoporous nanoparticles on dentin and its ability to inhibit *Enterococcus faecalis*. *J Mater Sci Mater Med*. 2016;27(1):16.